A Safety Enhanced, High Step-Up DC–DC Converter for AC Photovoltaic Module Application

Shih-Ming Chen, *Student Member, IEEE*, Tsorng-Juu Liang, *Senior Member, IEEE*, Lung-Sheng Yang, and Jiann-Fuh Chen, *Member, IEEE*

***Abstract*—Within the photovoltaic (PV) power-generation market, the ac PV module has shown obvious growth. However, a high voltage gain converter is essential for the module's grid connection through a dc–ac inverter. This paper proposes a converter that employs a floating active switch to isolate energy from the PV panel when the ac module is OFF; this particular design protects installers and users from electrical hazards. Without extreme duty ratios and the numerous turns-ratios of a coupled inductor, this converter achieves a high step-up voltage-conversion ratio; the leakage inductor energy of the coupled inductor is efficiently recycled to the load. These features explain the module's high-efficiency performance. The detailed operating principles and steady-state analyses of continuous, discontinuous, and boundary conduction modes are described. A 15 V input voltage, 200 V output voltage, and 100 W output power prototype circuit of the proposed converter has been implemented; its maximum efficiency is up to 95.3% and full-load efficiency is 92.3%.**

***Index Terms*—AC module, coupled inductor, high step-up voltage gain, single switch.**

I. Introduction

PHOTOVOLTAIC (PV) power-generation systems are becoming increasingly important and prevalent in distribution generation systems. A conventional centralized PV array is a serial connection of numerous panels to obtain higher dc-link voltage for main electricity through a dc–ac inverter [1], [30]. Unfortunately, once there is a partial shadow on some panels, the system's energy yield becomes significantly reduced [2]. An ac module is a microinverter configured on the rear bezel of a PV panel [1]–[3]; this alternative solution not only immunizes against the yield loss by shadow effect, but also provides flexible installation options in accordance with the user's budget [4]. Many prior research works have proposed a single-stage dc–ac inverter with fewer components to fit the dimensions of the bezel of the ac module, but their efficiency levels are lower than those of conventional PV inverters. The power capacity range of a single PV panel is about 100 W to 300 W, and the maximum power point (MPP) voltage range is from 15 V to 40 V, which will be the input voltage of the ac module; in cases with lower input voltage, it is difficult for the ac module to reach high efficiency [3]. However, employing a high step-up dc–dc converter in the front of the inverter improves power-conversion efficiency and provides a stable dc link to the inverter.

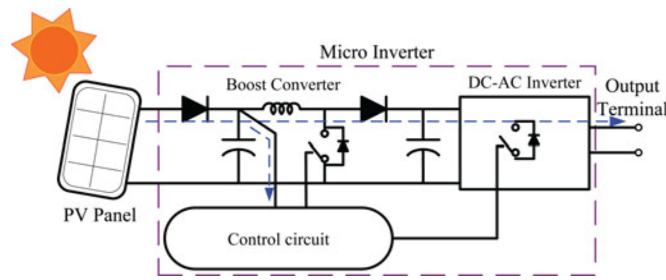

Fig. 1. Potential difference on the output terminal of nonfloating switch microinverter.

When installing the PV generation system during daylight, for safety reasons, the ac module outputs zero voltage [4], [5]. Fig. 1 shows the solar energy through the PV panel and micro inverter to the output terminal when the switches are OFF. When installation of the ac module is taking place, this potential difference could pose hazards to both the worker and the facilities. A floating active switch is designed to isolate the dc current from the PV panel, for when the ac module is off-grid as well as in the nonoperating condition. This isolation ensures the operation of the internal components without any residential energy being transferred to the output or input terminals, which could be unsafe.

The microinverter includes dc–dc boost converter, dc–ac inverter with control circuit as shown in Fig. 1. The dc–dc converter requires large step-up conversion from the panel's low voltage to the voltage level of the application. Previous research on various converters for high step-up applications has included analyses of the switched-inductor and switched-capacitor types [6], [7]; transformerless switched-capacitor type [8], [9], [29]; the voltage-lift type [12]; the capacitor-diode voltage multiplier [13]; and the boost type integrated with a coupled inductor [10], [11], these converters by increasing turns ratio of coupled inductor obtain higher voltage gain than conventional boost converter. Some converters successfully combined boost and flyback converters, since various converter combinations are developed to carry out high step-up voltage gain by using the coupled-inductor technique [14]–[19], [27], [28]. The efficiency and voltage gain of the dc–dc boost converter are constrained by

Manuscript received January 27, 2011; revised April 18, 2011 and July 5, 2011; accepted September 12, 2011. Date of current version February 20, 2012. This work was supported by the National Science Council of Taiwan, under project No. NSC 99-2218-E-006-004. Recommended for publication by Associate Editor T. Shimizu.

S.-M. Chen, T.-J. Liang, and J.-F. Chen are with the Green Energy Electronics Research Center (GEERC), Department of Electrical Engineering, National Cheng Kung University, Tainan, Taiwan (e-mail: orion.chen@msa.hinet.net, tjliang@mail.ncku.edu.tw, chenjf@mail.ncku.edu.tw).

L.-S. Yang is with the Department of Electrical Engineering, Far East University, Tainan, Taiwan (e-mail: yanglungsheng@yahoo.com.tw).

Color versions of one or more of the figures in this paper are available online at http://ieeexplore.ieee.org.

Digital Object Identifier 10.1109/TPEL.2011.2170097

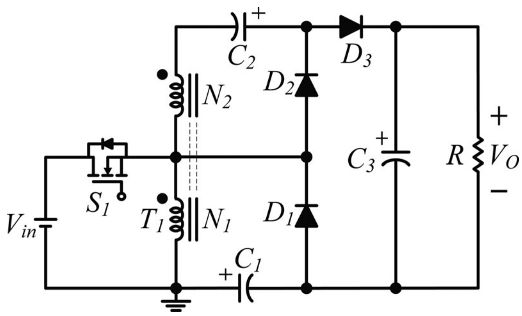

Fig. 2. Circuit configuration of proposed converter.

either the parasitic effect of the power switches or the reverse-recovery issue of the diodes. In addition, the equivalent series resistance (ESR) of the capacitor and the parasitic resistances of the inductor also affect overall efficiency. Use of active clamp technique not only recycles the leakage inductor's energy but also constrains the voltage stress across the active switch, however the tradeoff is higher cost and complex control circuit [25], [26]. By combining active snubber, auxiliary resonant circuit, synchronous rectifiers, or switched- capacitor-based resonant circuits and so on, these techniques made active switch into zero voltage switching (ZVS) or zero current switching (ZCS) operation and improved converter efficiency [20]–[24]. However, when the leakage-inductor energy from the coupled inductor can be recycled, the voltage stress on the active switch is reduced, which means the coupled inductor employed in combination with the voltage-multiplier or voltage-lift technique successfully accomplishes the goal of higher voltage gain [6]–[13].

The proposed converter, shown in Fig. 2, is comprised of a coupled inductor T_1 with the floating active switch S_1. The primary winding N_1 of a coupled inductor T_1 is similar to the input inductor of the conventional boost converter, and capacitor C_1 and diode D_1 receive leakage inductor energy from N_1. The secondary winding N_2 of coupled inductor T_1 is connected with another pair of capacitors C_2 and diode D_2, which are in series with N_1 in order to further enlarge the boost voltage. The rectifier diode D_3 connects to its output capacitor C_3. The proposed converter has several features: 1) The connection of the two pairs of inductors, capacitor, and diode gives a large step-up voltage-conversion ratio; 2) the leakage-inductor energy of the coupled inductor can be recycled, thus increasing the efficiency and restraining the voltage stress across the active switch; and 3) the floating active switch efficiently isolates the PV panel energy during nonoperating conditions, which enhances safety. The operating principles and steady-state analysis of the proposed converter are presented in the following sections.

II. Operating Principles of the Proposed Converter

The simplified circuit model of the proposed converter is shown in Fig. 3. The coupled inductor T_1 is represented as a magnetizing inductor L_m, primary and secondary leakage inductors L_{k1} and L_{k2}, and an ideal transformer. In order to simplify the circuit analysis of the proposed converter, the following assumptions are made.

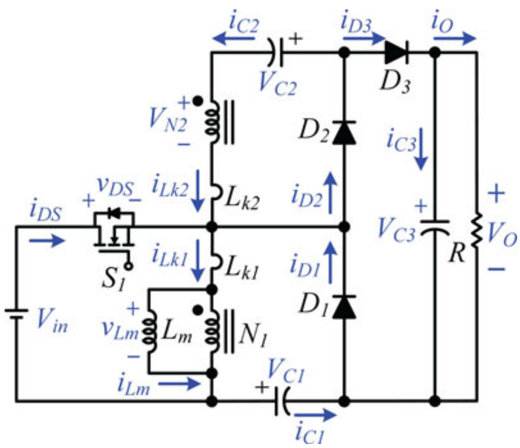

Fig. 3. Polarity definitions of voltage and current in proposed converter.

1) All components are ideal, except for the leakage inductance of coupled inductor T_1, which is being taken under consideration. The on-state resistance $R_{\mathrm{DS(ON)}}$ and all parasitic capacitances of the main switch S_1 are neglected, as are the forward voltage drops of diodes $D_1 \sim D_3$.
2) The capacitors $C_1 \sim C_3$ are sufficiently large that the voltages across them are considered to be constant.
3) The ESR of capacitors $C_1 \sim C_3$ and the parasitic resistance of coupled inductor T_1 are neglected.
4) The turns ratio n of the coupled inductor T_1 windings is equal to N_2/N_1.

The operating principle of continuous conduction mode (CCM) is presented in detail. The current waveforms of major components are given in Fig. 4. There are five operating modes in a switching period. The operating modes are described as follows.

A. CCM Operation

Mode I [t_0, t_1]: In this transition interval, the magnetizing inductor L_m continuously charges capacitor C_2 through T_1 when S_1 is turned ON. The current flow path is shown in Fig. 5(a); switch S_1 and diode D_2 are conducting. The current i_{Lm} is decreasing because source voltage V_{in} crosses magnetizing inductor L_m and primary leakage inductor L_{k1}; magnetizing inductor L_m is still transferring its energy through coupled inductor T_1 to charge switched capacitor C_2, but the energy is decreasing; the charging current i_{D2} and i_{C2} are decreasing. The secondary leakage inductor current i_{LK2} is declining as equal to i_{Lm} / n. Once the increasing i_{Lk1} equals decreasing i_{Lm} at $t = t_1$, this mode ends.

Mode II [t_1, t_2]: During this interval, source energy V_{in} is series connected with N_2, C_1 , and C_2 to charge output capacitor C_3 and load R; meanwhile magnetizing inductor L_m is also receiving energy from V_{in}. The current flow path is shown in Fig. 5(b), where switch S_1 remains ON, and only diode D_3 is conducting. The i_{Lm}, i_{Lk1}, and i_{D3} are increasing because the V_{in} is crossing L_{k1}, L_m, and primary winding N_1; L_m and L_{k1} are storing energy from V_{in}; meanwhile V_{in} is also serially connected with secondary winding N_2 of coupled inductor

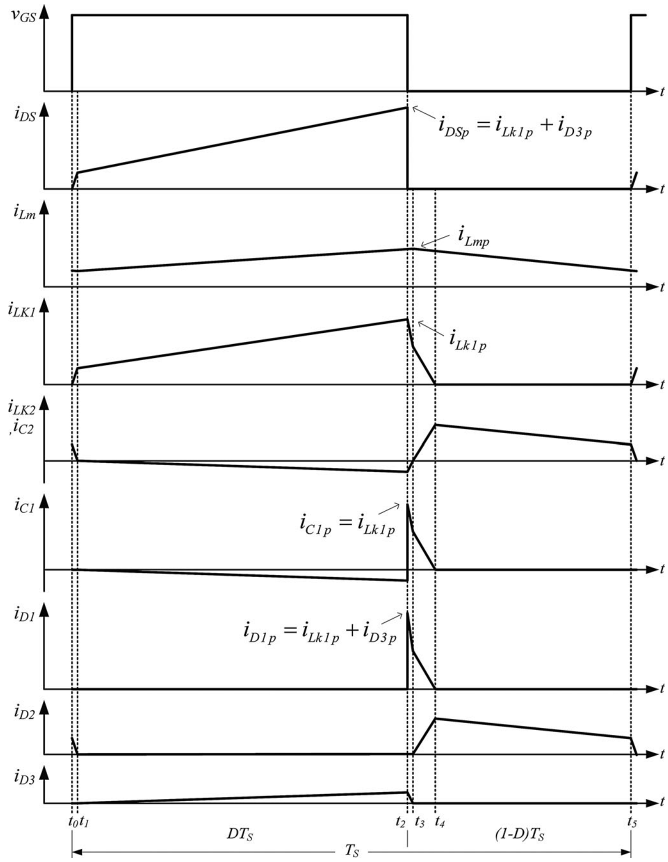

Fig. 4. Some typical waveforms of proposed converters at CCM operation.

T_1, capacitors C_1, and C_2, and then discharges their energy to capacitor C_3 and load R. The $i_{\rm in}$, i_{D3} and discharging current $|i_{C1}|$ and $|i_{C2}|$ are increasing. This mode ends when switch S_1 is turned OFF at $t = t_2$.

Mode III [t_2, t_3]: During this transition interval, secondary leakage inductor L_{k2} keeps charging C_3 when switch S_1 is OFF. The current flow path is shown in Fig. 5(c), where only diode D_1 and D_3 are conducting. The energy stored in leakage inductor L_{k1} flows through diode D_1 to charge capacitor C_1 instantly when S_1 is OFF. Meanwhile, the energy of secondary leakage inductor L_{k2} is series connected with C_2 to charge output capacitor C_3 and the load. Because leakage inductance L_{k1} and L_{K2} are far smaller than L_m, i_{Lk2} rapidly decreases, but i_{Lm} is increasing because magnetizing inductor L_m is receiving energy from L_{k1}. Current i_{Lk2} decreases until it reaches zero; this mode ends at $t = t_3$.

Mode IV [t_3, t_4]: During this transition interval, the energy stored in magnetizing inductor L_m is released to C_1 and C_2 simultaneously. The current flow path is shown in Fig. 5(d). Only diodes D_1 and D_2 are conducting. Currents i_{Lk1} and i_{D1} are continually decreased because the leakage energy still flowing through diode D_1 keeps charging capacitor C_1. The L_m is delivering its energy through T_1 and D_2 to charge capacitor C_2. The energy stored in capacitor C_3 is constantly discharged to the load R. These energy transfers result in decreases in i_{Lk1} and i_{Lm} but increases in i_Lk_2. This mode ends when current i_{Lk1} is zero, at $t = t_4$.

Mode V [t_4, t_5]: During this interval, only magnetizing inductor L_m is constantly releasing its energy to C_2. The current flow path is shown in Fig. 5(e), in which only diode D_2 is conducting. The i_{Lm} is decreasing due to the magnetizing inductor energy flowing through the coupled inductor T_1 to secondary winding N_2, and D_2 continues to charge capacitor C_2. The energy stored in capacitor C_3 is constantly discharged to the load R. This mode ends when switch S_1 is turned ON at the beginning of the next switching period.

B. DCM Operation

The detailed operating principles for discontinuous-conduction-mode (DCM) operation are presented in this section. Fig. 6 depicts several typical waveforms during five operating modes of one switching period. The operating modes are described as follows.

Mode I [t_0, t_1]: During this interval, source energy $V_{\rm in}$ is series connected with N_2, C_1, and C_2 to charge output capacitor C_3 and load R; meanwhile, magnetizing inductor L_m is also receiving energy from $V_{\rm in}$. The current flow path is shown in Fig. 7(a), which depicts that switch S_1 remains ON, and only diode D_3 is conducting. The i_{Lm}, i_{Lk1}, and i_{D3} are increasing because the $V_{\rm in}$ is crossing L_{k1}, L_m, and primary winding N_1; L_m and L_{k1} are storing energy from $V_{\rm in}$; meanwhile, $V_{\rm in}$ also is serially connected with secondary winding N_2 of coupled inductor T_1, capacitors C_1, and C_2; then they all discharge their energy to capacitor C_3 and load R. The $i_{\rm in}$, i_{D3} and discharging current $|i_{C1}|$ and $|i_{C2}|$ are increasing. This mode ends when switch S_1 is turned OFF at $t = t_1$.

Mode II [t_1, t_2]: During this transition interval, secondary leakage inductor L_{k2} keeps charging C_3 when switch S_1 is OFF. The current flow path is shown in Fig. 7(b), and only diode D_2 and D_3 are conducting. The energy stored in leakage inductor L_{k1} flows through diode D_1 to charge capacitor C_1 instantly when S_1 is OFF. Meanwhile, the energy of secondary leakage inductor L_{k2} is series-connected with C_2 to charge output capacitor C_3 and the load. Because leakage inductance L_{k1} and L_{K2} are far smaller than L_m, i_{Lk2} decreases rapidly, but i_{Lm} is increasing because magnetizing inductor L_m is receiving energy from L_{k1}. Current i_{Lk2} reduces down to zero, and this mode ends at $t = t_2$.

Mode III [t_2, t_3]: During this transition interval, the energy stored in coupled inductor T_1 is releasing to C_1 and C_2. The current flow path is shown in Fig. 7(c). Only diodes D_1 and D_2 are conducting. Currents i_{Lk1} and i_{D1} are continually decreased because leakage energy still flowing through diode D_1 keeps charging capacitor C_1. The L_m is delivering its energy through T_1 and D_2 to charge capacitor C_2. The energy stored in capacitor C_3 is constantly discharged to the load R. These energy transfers result in decreases in i_{Lk1} and i_{Lm} but increases in i_{Lk2}. This mode ends when current i_{Lk1} reaches zero at $t = t_3$.

Mode IV [t_3, t_4]: During this interval, only magnetizing inductor L_m is constantly releasing its energy to C_2. The current flow path is shown in Fig. 7(d), and only diode D_2 is conducting.

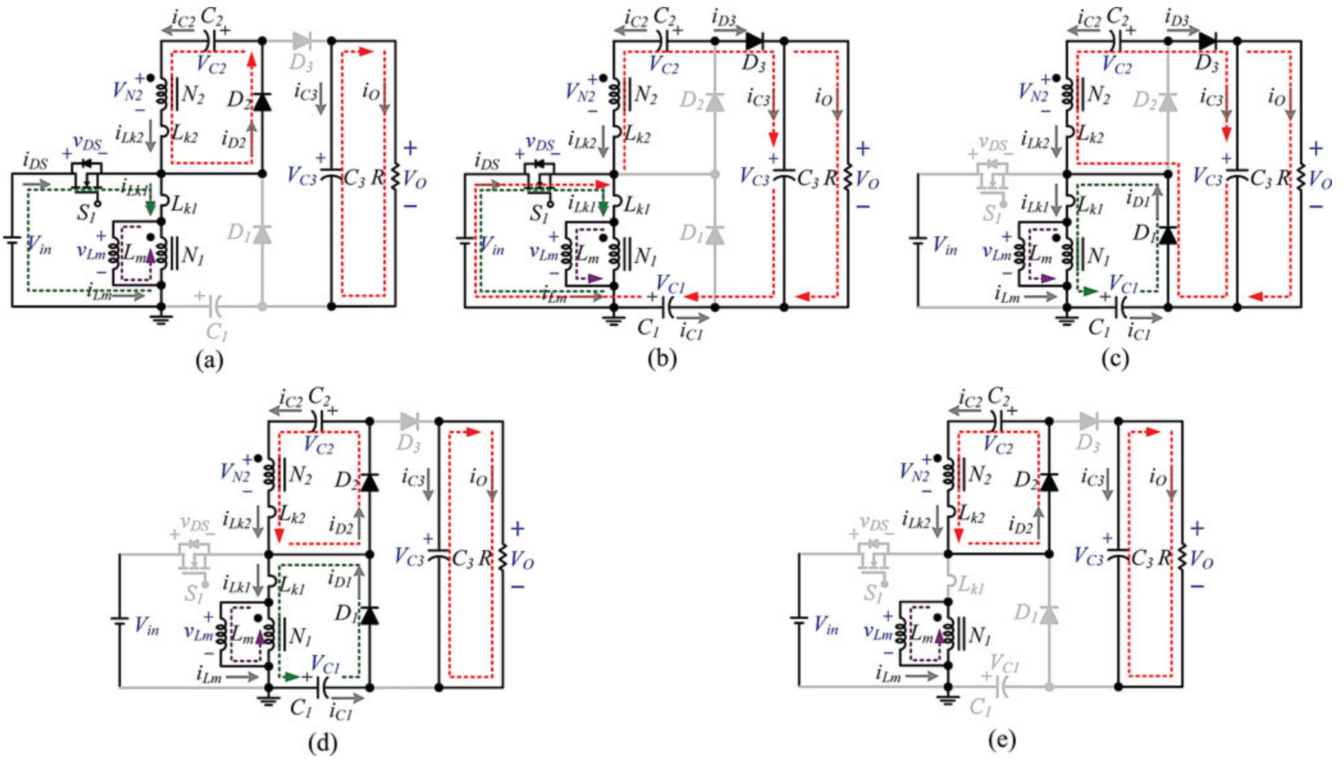

Fig. 5. Current flow path of five operating modes during one switching period at CCM operation. (a) Mode I: $t_0 \sim t_1$. (b) Mode II: $t_1 \sim t_2$. (c) Mode III: $t_2 \sim t_3$. (d) Mode IV: $t_3 \sim t_4$. (e) Mode V: $t_4 \sim t_5$.

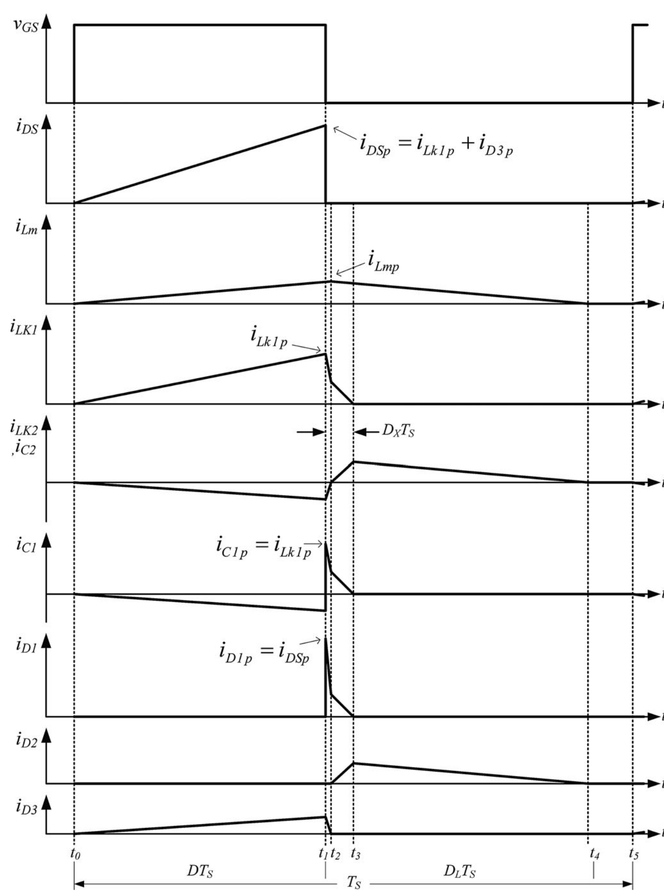

Fig. 6. Some typical waveforms of proposed converters at DCM operation.

The i_{Lm} is decreasing due to the magnetizing inductor energy flowing through the coupled inductor T_1 to secondary winding N_2, and D_2 continues to charge capacitor C_2. The energy stored in capacitor C_3 is constantly discharged to the load R. This mode ends when current i_{Lm} reaches zero at $t = t_4$.

Mode V [t_4, t_5]: During this interval, all active components are turned OFF; only the energy stored in capacitor C_3 is continued to be discharged to the load R. The current flow path is shown in Fig. 7(e). This mode ends when switch S_1 is turned ON at the beginning of the next switching period.

III. Steady-State Analysis of Proposed Converters

A. CCM Operation

To simplify the steady-state analysis, only modes II and IV are considered for CCM operation, and the leakage inductances on the secondary and primary sides are neglected. The following equations can be written from Fig. 5(b):

$$v_{Lm} = V_{\text{in}} \tag{1}$$

$$v_{N2} = nV_{\text{in}}. \tag{2}$$

During mode IV

$$v_{Lm} = -V_{C1} \tag{3}$$

$$v_{N2} = -V_{C2}. \tag{4}$$

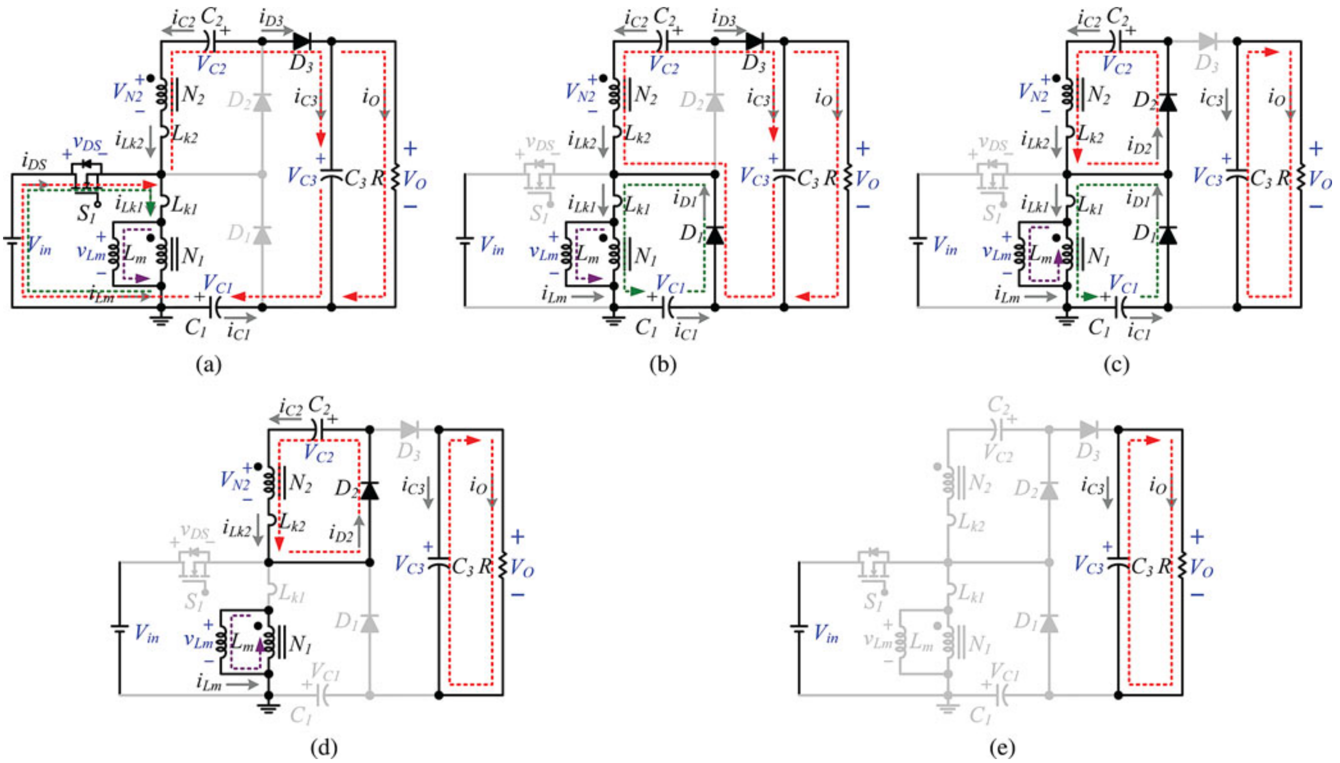

Fig. 7. Current flow path of five operating modes during one switching period at DCM operation. (a) Mode I: $t_0 \sim t_1$. (b) Mode II: $t_1 \sim t_2$. (c) Mode III: $t_2 \sim t_3$. (d) Mode IV: $t_3 \sim t_4$. (e) Mode V: $t_4 \sim t_5$.

Applying a volt-second balance on the magnetizing inductor L_m yields

$$\int_0^{DT_S} (V_{\text{in}})dt + \int_{DT_S}^{T_S} (-V_{C1})dt = 0 \tag{5}$$

$$\int_0^{DT_S} (nV_{\text{in}})dt + \int_{DT_S}^{T_S} (-V_{C2})dt = 0 \tag{6}$$

from which the voltage across capacitors C_1 and C_2 are obtained as follows:

$$V_{C1} = \frac{D}{1-D}V_{\text{in}} \tag{7}$$

$$V_{C2} = \frac{nD}{1-D}V_{\text{in}}. \tag{8}$$

During mode II, the output voltage $V_O = V_{\text{in}} + V_{N2} + V_{C2} + V_{C1}$ becomes

$$V_{\text{O}} = V_{\text{in}} + nV_{\text{in}} + \frac{nD}{1-D}V_{\text{in}} + \frac{D}{1-D}V_{\text{in}}. \tag{9}$$

The DC voltage gain $\mathrm{M_{CCM}}$ can be found as follows:

$$M_{\text{CCM}} = \frac{\mathrm{V_O}}{V_{\text{in}}} = \frac{1+n}{1-D}. \tag{10}$$

Both [10] and [11] are employing coupled inductor topology as the boost type converter integrating with coupled inductor; this technology is similar to the technology of the proposed converter. Fig. 8 shows the plot of voltage gain M_{CCM} as function of duty ratio D of the proposed converter is compared with that of available converters [10], [11]. The chart reveals the voltage gain M_{CCM} of proposed converter is obviously higher than available converters. All of them are operating under the same conditions: CCM and $n = 5$.

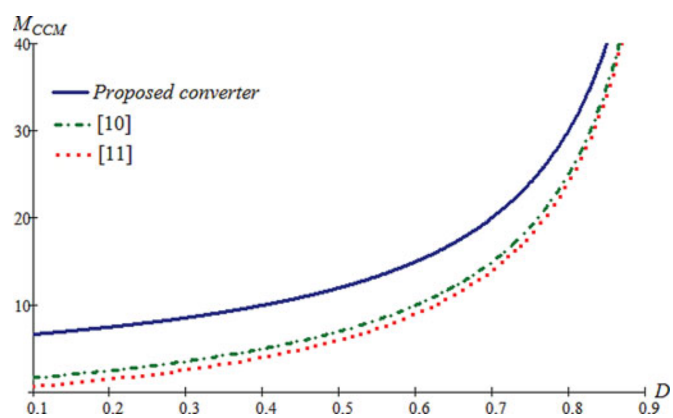

Fig. 8. Voltage gain as a function of the duty ratio of the proposed converter. [10] and [11] under CCM operation and $n = 5$.

During CCM operation, the voltage stresses on S_1 and $D_1 \sim D_3$ are given as

$$V_{\text{DS}} = V_{D1} = \frac{V_{\text{in}}}{1-D} \tag{11}$$

$$V_{D2} = \frac{nV_{\text{in}}}{1-D} \tag{12}$$

$$V_{D3} = \frac{1+n}{1-D}V_{\text{in}}. \tag{13}$$

B. DCM Operation

To simplify the steady-state analysis, only modes I and IV are considered for DCM operation, and the leakage inductances on the secondary and primary sides are neglected. The following equations can be written from Fig. 7(a). When switch S_1 is turned ON, the voltage levels across inductors L_m and secondary winding N_2 are

$$V_{Lm} = V_{\rm in} \tag{14}$$

$$v_{N2} = nV_{\rm in}. \tag{15}$$

When switch S_1 is turned OFF, the voltage levels across inductors L_m and secondary winding N_2 are

$$v_{Lm} = -V_{C1} \tag{16}$$

$$-v_{N2} = V_{C2}. \tag{17}$$

$D_L T_S$ is the period of time during which current i_{Lm} declines from peak current to zero. The voltage across L_m and secondary winding N_2 can be found, as follows, by using the volt-second balance principle

$$\int_0^{DT_S} V_{\rm in} dt + \int_{DT_S}^{(D+D_L)T_S} (-V_{C1}) dt = 0 \tag{18}$$

$$\int_0^{DT_S} (nV_{\rm in}) dt + \int_{DT_S}^{(D+D_L)T_S} (-V_{C2}) dt = 0 \tag{19}$$

which derives the voltage of C_3, C_4, and output voltage as

$$V_{C1} = \frac{D}{D_L} V_{\rm in} \tag{20}$$

$$V_{C2} = \frac{nD}{D_L} V_{\rm in} \tag{21}$$

$$V_O = \frac{(n+1)(D+D_L)}{D_L} V_{\rm in}. \tag{22}$$

Equation (22) yields D_L as follows:

$$D_L = \frac{(n+1)D}{(V_O/V_{\rm in}) - (n+1)}. \tag{23}$$

Since the average currents of capacitor I_{C1}, I_{C2}, and I_{C3} are zero in steady state, the average current values for I_{D3}, I_{D2}, and I_{D1} are, respectively, equal to the average value of I_O. The $I_{\rm Lmp}$ is the peak current of the magnetizing inductor, as shown in the following:

$$I_{\rm Lmp} = \frac{V_{\rm in} D T_S}{L_m}. \tag{24}$$

From Fig. 6, the average values for D_1 and D_2 are derived as

$$I_{D1} = \frac{(1/2) I_{\rm Lmp} D_X T_S}{T_S} \tag{25}$$

$$I_O = I_{D2} = \frac{I_{\rm Lmp}(D_L - D_X)T_S}{2nT_S}. \tag{26}$$

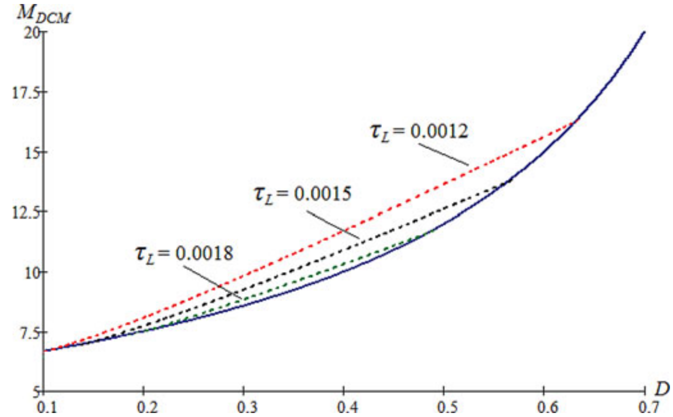

Fig. 9. Voltage gain as a function of the duty ratio of the proposed converter under DCM operation with different τ_L by $n = 5$.

Since the average current values for I_{D2} and I_{D1} are, respectively, equal to the average value of I_O (25) is equal to (26), D_X, which is defined as the duration during which diode current i_{D1} travels from peak down to zero, is

$$D_X = \frac{D_L}{n+1}. \tag{27}$$

Then, substituting (27) into (26), the I_O can be rewritten as

$$I_O = \frac{D_L I_{\rm Lmp}}{2(n+1)}. \tag{28}$$

Since $I_O = V_O / R$, substituting (24) and (27) into (28) yields

$$\frac{2D}{(V_O/V_{\rm in}) - (n+1)} \cdot \frac{V_{\rm in}}{V_O} D = \frac{L_m}{RT_S}. \tag{29}$$

The normalized magnetizing inductor time constant τ_L is defined as

$$\tau_L = \frac{L_m}{RT_S} = \frac{L_m f_S}{R} \tag{30}$$

where f_S is the switching frequency. Substituting (30) into (29) obtains the voltage gain of the proposed converter in DCM, as follows:

$$M_{\rm DCM} = \frac{V_O}{V_{\rm in}} = \frac{(n+1) + \sqrt{(n+1)^2 + (2D^2/\tau_L)}}{2}. \tag{31}$$

Equation (31) can be used to illustrate DCM voltage gain lines by different magnetizing inductor time constants τ_L, as shown in Fig. 9.

C. BCM Condition

When the proposed converter is operating in boundary conduction mode (BCM), the voltage gains of CCM and DCM operation are equal. Using (10) and (31) allows boundary

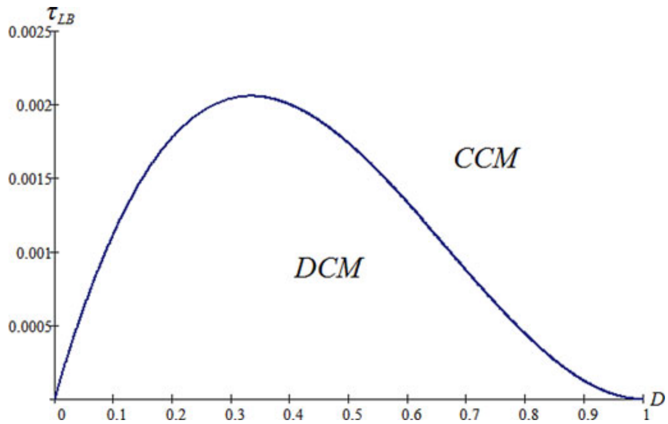

Fig. 10. Boundary condition of $\tau_{\rm LB}$ of proposed converter under $n = 5$.

normalized magnetizing inductor time constant $\tau_{\rm LB}$ to be depicted as

$$\tau_{\rm LB} = \frac{D(1-D)^2}{2(1+n)^2} = \frac{D}{2(M_{\rm CCM})^2}. \qquad (32)$$

The curve of $\tau_{\rm LB}$ is plotted in Fig. 10. Once the τ_{Lm} is higher than boundary curve $\tau_{\rm LmB}$, the proposed converter operates in CCM.

IV. Experimental Results

A 100 W prototype sample is presented to verify the practicability of the proposed converter. The electrical specifications are $V_{\rm in} = 15$ V, $V_O = 200$ V, $f_S = 50$ kHz, and full-load resistance $R = 400\ \Omega$. The major components required are $C_1 = C_2 = 47\ \mu$F and $C_3 = 220\ \mu$F. The main switch S_1 is a MOSFET IXFK180N15P, the diodes D_1 are MRB20200CTG, and the DPG30C300HB is selected for D_2 and D_3. Since (10) assign turns ratio $n = 5$, the duty ratio D is derived as 55%.

The boundary normalized magnetizing inductor time constant $\tau_{\rm LB}$ is found by (28) to be 1.547×10^{-3}. To define the proposed converter's BCM operation at 50% of the full load, the load resistance $R = 800\ \Omega$. The boundary magnetizing inductance $L_{\rm mB}$ is found as follows:

$$\frac{L_{\rm mB} \cdot f_S}{R} > 1.547 * 10^{-3} \Rightarrow L_m > 24.75\ \mu\text{H}. \qquad (33)$$

The actual inductance of magnetizing inductor L_m of the coupled inductor is 30.54 μH, which is larger than boundary magnetizing inductance 24.75 μH. Fig. 11 shows voltage and current waveforms, which are measured from active switch S_1, diodes D_1, D_2, and D_3, and the current waveforms of C_1 and C_2. The measured voltage spike across the active switch is found to be about 80 V; this reveals that the energy of the leakage inductor has been stored in and voltage clamped by C_1. These experimental waveforms agree with the operating principles and the steady-state analysis. Fig. 12 shows that the maximum efficiency of 95.3% occurred at 40% of full load; and the full-load efficiency is maintained at 92.3%. The efficiency variation is about 3%, and the flat efficiency curve is able to yield higher energy from the PV module during periods when sunlight is

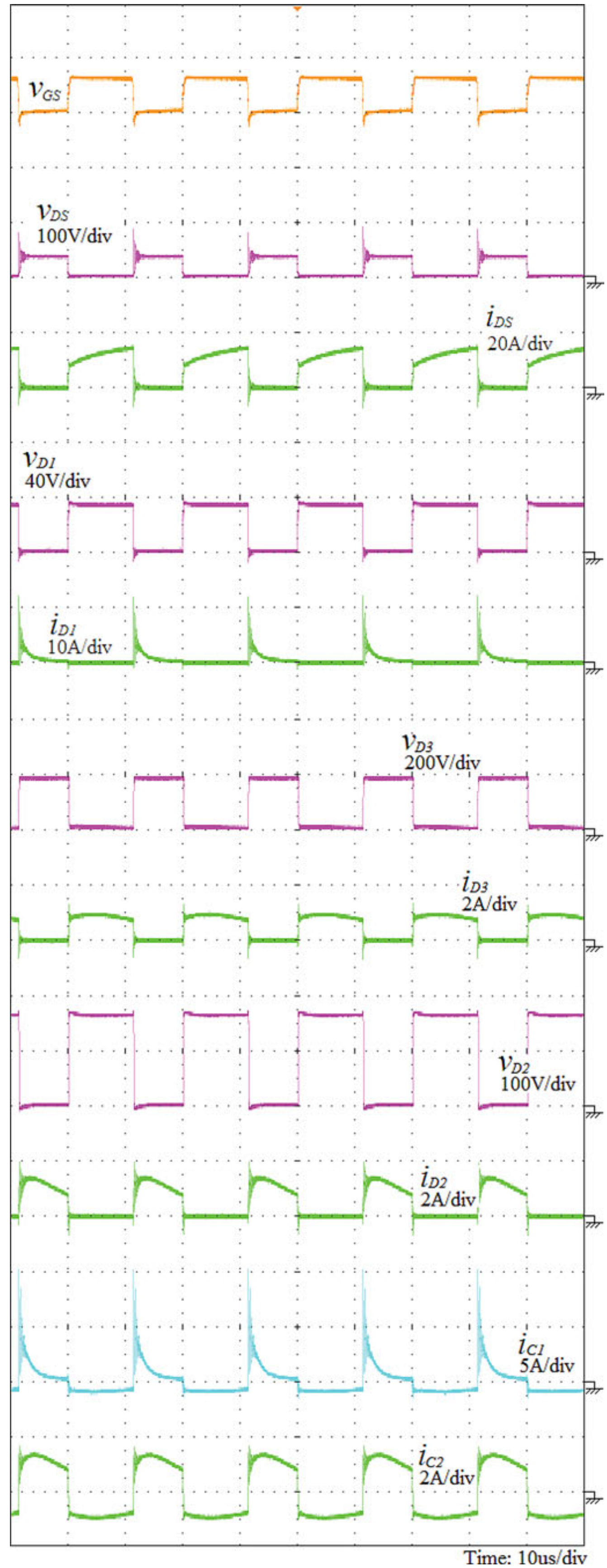

Fig. 11. Experimental waveforms measured by the condition of $f_S = 50$ kHz, $V_{\rm in} = 15$ V, and output 100 W.

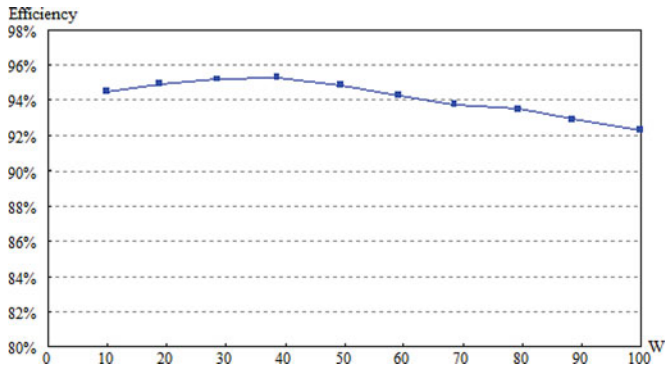

Fig. 12. Measured efficiency of proposed converter.

fading. The residential voltage discharge time of the proposed converter is 480 milliseconds, which prevents any potential electrical injuries to humans.

V. Conclusion

Since the energy of the coupled inductor's leakage inductor has been recycled, the voltage stress across the active switch S_1 is constrained, which means low ON-state resistance $R_{\mathrm{DS(ON)}}$ can be selected. Thus, improvements to the efficiency of the proposed converter have been achieved. The switching signal action is performed well by the floating switch during system operation; on the other hand, the residential energy is effectively eliminated during the nonoperating condition, which improves safety to system technicians. From the prototype converter, the turns ratio $n = 5$ and the duty ratio D is 55%; thus, without extreme duty ratios and turns ratios, the proposed converter achieves high step-up voltage gain, of up to 13 times the level of input voltage. The experimental results show that the maximum efficiency of 95.3% is measured at half load, and a small efficiency variation will harvest more energy from the PV module during fading sunlight.

References

[1] T. Shimizu, K. Wada, and N. Nakamura, "Flyback-type single-phase utility interactive inverter with power pulsation decoupling on the dc input for an ac photovoltaic module system," *IEEE Trans. Power Electron.*, vol. 21, no. 5, pp. 1264–1272, Jan. 2006.

[2] C. Rodriguez and G. A. J. Amaratunga, "Long-lifetime power inverter for photovoltaic ac modules," *IEEE Trans. Ind. Electron.*, vol. 55, no. 7, pp. 2593–2601, Jul. 2008.

[3] S. B. Kjaer, J. K. Pedersen, and F. Blaabjerg, "A review of single-phase grid-connected inverters for photovoltaic modules," *IEEE Trans. Ind. Appl.*, vol. 41, no. 5, pp. 1292–1306, Sep./Oct. 2005.

[4] J. J. Bzura, "The ac module: An overview and update on self-contained modular PV systems," in *Proc. IEEE Power Eng. Soc. Gen. Meeting*, Jul. 2010, pp. 1–3.

[5] B. Jablonska, A. L. Kooijman-van Dijk, H. F. Kaan, M. van Leeuwen, G. T. M. de Boer, and H. H. C. de Moor, "PV-PRIVÉ project at ECN, five years of experience with small-scale ac module PV systems," in *Proc. 20th Eur. Photovoltaic Solar Energy Conf.*, Barcelona, Spain, Jun. 2005, pp. 2728–2731.

[6] T. Umeno, K. Takahashi, F. Ueno, T. Inoue, and I. Oota, "A new approach to low ripple-noise switching converters on the basis of switched- capacitor converters," in *Proc. IEEE Int. Symp. Circuits Syst.*, Jun. 1991, pp. 1077–1080.

[7] B. Axelrod, Y. Berkovich, and A. Ioinovici, "Switched-capacitor/ switched-inductor structures for getting transformerless hybrid dc–dc PWM converters," *IEEE Trans. Circuits Syst. I, Reg. Papers*, vol. 55, no. 2, pp. 687–696, Mar. 2008.

[8] B. Axelrod, Y. Berkovich, and A. Ioinovici, "Transformerless dc–dc converters with a very high dc line-to-load voltage ratio," in *Proc. IEEE Int. Symp. Circuits Syst. (ISCAS)*, 2003, vol. 3, pp. 435–438.

[9] H. Chung and Y. K. Mok, "Development of a switched-capacitor dc–dc boost converter with continuous input current waveform," *IEEE Trans. Circuits Syst. I, Fundam. Theory Appl.*, vol. 46, no. 6, pp. 756–759, Jun. 1999.

[10] T. J. Liang and K. C. Tseng, "Analysis of integrated boost-flyback step-up converter," *IEE Proc. Electrical Power Appl.*, vol. 152, no. 2, pp. 217–225, Mar. 2005.

[11] Q. Zhao and F. C. Lee, "High-efficiency, high step-up dc–dc converters," *IEEE Trans. Power Electron.*, vol. 18, no. 1, pp. 65–73, Jan. 2003.

[12] M. Zhu and F. L. Luo, "Voltage-lift-type cuk converters: Topology and analysis," *IET Power Electron.*, vol. 2, no. 2, pp. 178–191, Mar. 2009.

[13] J. W. Baek, M. H. Ryoo, T. J. Kim, D. W. Yoo, and J. S. Kim, "High boost converter using voltage multiplier," in *Proc. IEEE Ind. Electron. Soc. Conf. (IECON)*, 2005, pp. 567–572.

[14] J. Xu, "Modeling and analysis of switching dc–dc converter with coupled-inductor," in *Proc. IEEE 1991 Int. Conf. Circuits Syst. (CICCAS)*, 1991, pp. 717–720.

[15] R. J. Wai, C. Y. Lin, R. Y. Duan, and Y. R. Chang, "High-efficiency dc–dc converter with high voltage gain and reduced switch stress," *IEEE Trans. Ind. Electron.*, vol. 54, no. 1, pp. 354–364, Feb. 2007.

[16] S. M. Chen, T. J. Liang, L. S. Yang, and J. F. Chen, "A cascaded high step-up dc–dc converter with single switch for microsource applications," *IEEE Trans. Power Electron.*, vol. 26, no. 4, pp. 1146–1153, Apr. 2011.

[17] T. J. Liang, S. M. Chen, L. S. Yang, J. F. Chen, and A. Ioinovici, "Ultra large gain step-up switched-capacitor dc–dc converter with coupled inductor for alternative sources of energy," *IEEE Trans. Circuits Syst. I*, to be published.

[18] L. S. Yang and T. J. Liang, "Analysis and implementation of a novel bidirectional dc–dc converter," *IEEE Trans. Ind. Electron.*, vol. 59, no. 1, pp. 422–434, Jan. 2012.

[19] W. Li and X. He, "Review of non-isolated high-step-up dc/dc converters in photovoltaic grid-connected applications," *IEEE Trans. Ind. Electron.*, vol. 58, no. 4, pp. 1239–1250, Apr. 2011.

[20] S. H. Park, S. R. Park, J. S. Yu, Y. C. Jung, and C. Y. Won, "Analysis and design of a soft-switching boost converter with an HI-Bridge auxiliary resonant circuit," *IEEE Trans. Power Electron.*, vol. 25, no. 8, pp. 2142–2149, Aug. 2010.

[21] G. Yao, A. Chen, and X. He, "Soft switching circuit for interleaved boost converters," *IEEE Trans. Power Electron.*, vol. 22, no. 1, pp. 80–86, Jan. 2007.

[22] Y. Park, S. Choi, W. Choi, and K. B. Lee, "Soft-switched interleaved boost converters for high step-up and high power applications," *IEEE Trans. Power Electron.*, vol. 26, no. 10, pp. 2906–2914, Oct. 2011.

[23] Y. Zhao, W. Li, Y. Deng, and X. He, "Analysis, design, and experimentation of an isolated ZVT boost converter with coupled inductors," *IEEE Trans. Power Electron.*, vol. 26, no. 2, pp. 541–550, Feb. 2011.

[24] H. Mao, O. Abdel Rahman, and I. Batarseh, "Zero-voltage-switching dc–dc converters with synchronous rectifiers," *IEEE Trans. Power Electron.*, vol. 23, no. 1, pp. 369–378, Jan. 2008.

[25] J. M. Kwon and B. H. Kwon, "High step-up active-clamp converter with input-current doubler and output-voltage doubler for fuel cell power systems," *IEEE Trans. Power Electron.*, vol. 24, no. 1, p. 108–115, Jan. 2009.

[26] S. Dwari and L. Parsa, "An efficient high-step-up interleaved dc–dc converter with a common active clamp," *IEEE Trans. Power Electron.*, vol. 26, no. 1, pp. 66–78, Jan. 2011.

[27] C. Restrepo, J. Calvente, A. Cid, A. El Aroudi, and R. Giral, "A non-inverting buck-boost dc–dc switching converter with high efficiency and wide bandwidth," *IEEE Trans. Power Electron.*, vol. 26, no. 9, pp. 2490–2503, Sep. 2011.

[28] K. B. Park, G. W. Moon, and M. J. Youn, "Nonisolated high step-up boost converter integrated with sepic converter," *IEEE Trans. Power Electron.*, vol. 25, no. 9, pp. 2266–2275, Sep. 2010.

[29] L. S. Yang, T. J. Liang, and J. F. Chen, "Transformerless dc–dc converters with high step-up voltage gain," *IEEE Trans. Ind. Electron.*, vol. 56, no. 8, pp. 3144–3152, Aug. 2009.

[30] N. Pogaku, M. Prodanovic, and T. C. Green, "Modeling, analysis and testing of autonomous operation of an inverter-based microgrid," *IEEE Trans. Power Electron.*, vol. 22, no. 2, pp. 613–625, Mar. 2007.

Shih-Ming (Orion) Chen (S'10) was born in Tainan, Taiwan, R.O.C. He received the B.S. and Ph.D. degrees in electrical engineering from National Cheng-Kung University, Tainan, Taiwan, in 2003 and 2011, respectively.

From 1991 to 1995, he was employed as a Research and Design Engineer at LUMIN Electronics, Taiwan. From 1995 to 1999, he was employed as a Section Manager of the Engineer Department at Delta Electronics, Inc., Taiwan. From 1999 to 2002, he was employed as a Manager-in-Charge of the Tainan R&D Center at Sino-American Electronic Co., Ltd., Taiwan. From 2002 to 2006, he has worked as a Section Manager at Product Development of LCD-TV Head Division, CHIMEI Optoelectronics Corp. Since 2009, he has rejoined Delta Electronics as Senior Manager in the division of LCD display power. Now, he is an Assistant Researcher of Green Energy Electronics Research Center (GEERC) in the Department of Electrical Engineering, National Cheng Kung University. His research interests include dc to dc converters, photovoltaic inverter, switching power supply, uninterrupted power system, CCFL/EEFL inverter design, and LED driver and chromatics control.

Tsorng-Juu (Peter) Liang (M'93–SM'10) was born in Kaohsiung, Taiwan, R.O.C. He received the B.S. degree in electrophysics from National Chiao-Tung University, Hsinchu, Taiwan, in 1985, and the M.S. and Ph.D. degrees in electrical engineering from the University of Missouri, Columbia, in 1990 and 1993, respectively.

He is currently a Professor of electrical engineering and Director of Green Energy Electronics Research Center (GEERC), National Cheng-Kung University (NCKU), Tainan, Taiwan. He was the Director of Electrical Laboratories at NCKU from 2001–2004. He is also on the Board of Directors for Compucase Enterprise Co., Ltd. and Catcher Technology Co., Ltd. He has authored or coauthored 50 journals, and more than 100 conference papers. His research interests include high efficiency power converters, high efficiency lighting systems, renewable energy conversion, and power ICs design.

Prof. Liang is a recipient of many outstanding awards and honors. In 2008, he received the Outstanding Engineer award from, The Chinese Institute of Electrical Engineering, Kaohsiung Chapter, and the Outstanding Professor Award from the, Taiwan Power Electronics Conference. In 2010, he received the Teaching Excellence Award from the, National Cheng Kung University and the Outstanding Engineers Professor Award from, The Chinese Institute of Electrical Engineering, Kaohsiung Branch. He is the Associate Editor of the IEEE TRANSACTIONS ON POWER ELECTRONICS, the Associate Editor of the IEEE TRANSACTIONS ON CIRCUITS AND SYSTEMS-I, and the Technical Committee Chair of IEEE CAS Systems Power and Energy Circuits and Systems Technical Committee. He is a member of the IEEE Societies of Power Electronics, Industrial Electronics, Circuits and System, and Industrial Applications.

Lung-Sheng Yang was born in Tainan, Taiwan, R.O.C., in 1967. He received the B.S. degree in electrical engineering from National Taiwan Institute of Technology, Taipei, Taiwan, in 1990, the M.S. degree in electrical engineering from National Tsing Hua University, Hsinchu, Taiwan, in 1992, and the Ph.D. degree in electrical engineering from National Cheng Kung University, Tainan, Taiwan, in 2007.

He is currently an Assistant Professor in the Department of Electrical Engineering, Far East University, Tainan, Taiwan. His research interests include power factor correction, dc–dc converters, renewable energy conversion, and electronic ballast.

Jiann-Fuh Chen (S'79–M'80) was born in Chung-Hua, Taiwan, R.O.C., in 1955. He received the B.S., M.S., and Ph.D. degrees in electrical engineering from National Cheng Kung University (NCKU), Tainan, Taiwan, in 1978, 1980, and 1985, respectively.

Since 1980, he has been with the Department of Electrical Engineering at (NCKU), Tainan, Taiwan, where he is currently a Professor. His research interests include power electronics and energy conversion.